SAND2020-9081J

Recovery from Plasma Etching-Induced Nitrogen Vacancies in p-type Gallium Nitride using UV/O_3 Treatments

Geoffrey M Foster[1*], Andrew Koehler[2], Mona Ebrish[3], James Gallagher[2], Travis Anderson[2], Brenton Noesges, Leonard Brillson[4,5], Brendan Gunning[6], Karl D. Hobart[2], Francis Kub[2]

[1]American Society for Engineering Education Postdoctoral Fellow Residing at U.S. Naval Research Laboratory, Washington, DC 20036, USA

[2] U.S. Naval Research Laboratory, Washington, DC 200375, USA

[3] National Research Council Postdoctoral Fellow Residing at the U.S. Naval Research Laboratory, Washington, DC 20036, USA

[4]Department of Physics, The Ohio State University, Columbus, Ohio 43210, USA

[5]Department of Electrical and Computer Engineering, The Ohio State University, Columbus, Ohio 43210, USA

[6] Sandia National Labs, Albuquerque, NM 87185, USA

*Correspond Author Email: geoffrey.foster.ctr@nrl.navy.mil

Abstract

Plasma etching of p-type GaN creates n-type nitrogen vacancy (V_N) defects at the etched surface, which can be detrimental to device performance. In mesa isolated diodes, etch damage on the sidewalls degrades the ideality factor and leakage current. A treatment was developed to recover both the ideality factor and leakage current, which uses UV/O_3 treatment to oxidize the damaged layers followed by HF etching to remove them. Temperature dependent I-V shows the reverse leakage transport mechanism is dominated by Poole-Frenkel emission at room temperature through the etch-induced V_N defect. Depth resolved cathodoluminescence confirms that the damage is limited to first several nanometers and is consistent with the V_N defect.

Gallium nitride (GaN) is a prime candidate for use in next generation power electronic devices. With recent advancements in the ability to grow reliably doped p-type GaN[1], pragmatic power devices can be realized, such as trench MOSFETs and mesa isolated PN diodes[2,3]. However, such devices require a plasma etch that can create damage, such as nitrogen vacancies which act as shallow donors[4–7]. N-type defects along the etched surface compensate the Mg acceptors in the p-GaN layer, leading to type conversion to n-type at the etched surface. This has the adverse effect of increasing leakage current along the etched sidewall, leading to premature breakdown, thus limiting device performance and reliability. The plasma etch damage must be eliminated to recover device performance. Wet chemical etches, such as KOH and TMAH, have commonly been used to treat plasma etched surfaces, and while these methods do in fact recover device performance, the etches can act on particular crystal faces, thus again limiting device performance[8–10]. Etch damage may also be removed, up to 500 A, by annealing at 750-900C.[11,12] Finally a UV/Ozone etch followed by an acid bath to remove the oxide layer, may also recover device performance[13]. The mechanisms behind the recovery have not been explored. This work examines and determines the exact mechanism to the recovery.

To investigate the effects of etch damage and recovery on plasma etched p-GaN sidewalls, a PN diode structure was grown on a native n-type GaN substrate. The epitaxial growth was performed by metalorganic chemical vapor deposition (MOCVD) in a Taiyo Nippon Sanso SR4000HT reactor at atmospheric pressure. The PN diode structure consisted of an 8 μm thick drift layer with a net electron concentration of 1.5×10^{16} cm^{-3}, 500 nm thick p-type GaN anode with Mg concentration of 2×10^{19} cm-3, and 15 nm thick p+ GaN contact layer with Mg concentration of 2×10^{20} cm^{-3}.

PN diodes were mesa isolated by a Cl_2/Ar inductively coupled plasma (ICP) reactive ion etch (RIE) for 8 min, etching 656 nm, to form 300 μm diameter mesas. The ICP-RIE conditions include a chamber pressure of 5 mTorr, a flow of 10 sccm Cl_2 and 5 sccm Ar, RF coil power of 40W, ICP substrate power of 150 W, and temperature of 25 °C. Then, 250 μm diameter Ohmic contacts to the p-type anode were formed by electron beam evaporation of Pd/Au and lift-off, and cathode Ohmics were formed by Ti/Al/Ni/Au[14]. Plasma etch damage cleanup was performed by subjecting the sample iteratively to a UV/O_3 treatment for 10 min at room temperature, followed by 2 min in 49% HF and then repeated for two total treatments. Two treatments were determined to have the most notable effect. Further treatments show slight improvement with diminishing returns. Pd/Au transmission line measurement (TLM) structures were also formed on separate unetched and etched surfaces, using a 5 min RIE etch. Subsurface plasma etch damage was characterized by forward and reverse current-voltage (I-V) characteristics, atomic force microscopy (AFM), ultra-violet photoluminescence (PL), and depth resolved cathodoluminescence spectroscopy (DRCLS).

Improvement in the diode performance is observed after UV/O_3 + HF treatment, as shown in Figure 1. In reverse bias, the leakage current decreases by nearly two orders of magnitude, and in forward bias, the diode ideality factor is lowered after treatment from 3.43 to 2.57[15]. The improvements are attributed to a reduction in shallow donors resulting from etch damage trap states. The activated p-GaN has a sheet resistance of 8.45 kΩ/□ with a specific contact resistance of 0.81 $m\Omega/cm^2$, as determined by TLM, after ICP-RIE, the contact resistance increases to 1.12 $m\Omega/cm^2$, likely caused by type conversion from p-type to n-type at the surface from a high density of shallow donor states. After UV/O_3 + HF treatment, the contact resistance was improved to lower the activated p-GaN with a contact resistance of 0.56 $m\Omega/cm^2$. The increased presence of surface donors from etch damage in the p-type material decreases its conductivity and makes it more difficult for the Pd to form an Ohmic contact. There are likely some surface defects present initially that are cleaned up in addition to the etch induced defects, leading to lowest contact resistance after the UV/O_3 + HF treatment. This same effect is also be observed in the photo- and cathodoluminescence.

Figure 1. The above shows IV characteristics before and after treatment of the mesa devices. Figure 1a. Shows the reverse current, which is a decrease in leakage after UV/O_3 + HF treatment. Figure 1b shows the forward conduction having a sharpening of the turn on characteristics, Figure 1c shows the ideality factor has been decreased after treatment through the entire turn on regime of 2-3V.

To determine the dominant transport mechanism responsible for leakage current in reverse bias, temperature dependent I-V measurements were performed[6] in a cryogenic probe station, with a reverse voltage of 0-70V. Many transport mechanisms show a dependence on either temperature or applied electric field. The log of the reverse leakage current density vs. voltage exhibits a linear dependence with temperature, implying that Poole-Frenkel emission (PFE) is the dominant transport mechanism for reverse bias leakage. Equation 1 describes the current density of PFE[6,16–18].

$$J = CE\ exp\left[-\frac{q(\phi_t - \sqrt{{qE}/{(\pi\varepsilon_o\varepsilon_{GaN})}}}{kT}\right] \tag{1}$$

where E is the electric field, ϕ_t is the barrier height for electron emission and ε_{GaN} is the relative dielectric permittivity at high frequency, ε_o is the permittivity of free space, T is the absolute temperature, q is the electron charge, and k is the Boltzmann constant.

Figure 2. The log plot of J/E shows a linear dependence in $E^{0.5}$ and an exponential dependence of temperature, showing that PFE is a dominant conduction mechanism in the reverse current.

From equation 1, current transport ruled by PFE should have a linear dependence between ln(J/E) and $E^{0.5}$. Figure 2 shows this linear dependence. With this linear dependence, ε_{GaN} and ϕ_t can be extracted by plotting the slopes and y-intercepts of Figure 2 as a function of temperature. Before UV/O_3 + HF treatment, the extracted ε_{GaN} and ϕ_t are found to be 8.19 and 0.79 eV respectively. After UV/O_3 + HF treatment, ε_{GaN} and ϕ_t are 8.59 and 0.78 eV respectively. The values for the permittivity agree well with values found in GaN (8.9 – 10.4). After treatment, the trap barrier height does not significantly change, indicating that the same trap level contributes to PFE responsible for leakage current. However, the main effect that is observed is a reduction in the reverse leakage current after UV/O_3 + HF treatment, indicating a reduction in the density of the defect with 0.78 eV trap barrier height. It should be noted that as the temperature decreases, the linearity of ln(J/E) v $E^{0.5}$ begins to deviate. This is because the dominant transport mechanism begins to change as the temperature decreases. Instead of being dominated only by PFE, other transport methods, including tunneling begin to play an increased role.

To study the effects of the plasma etch and recovery directly, surface roughness measurements were conducted by AFM. Initially, the as-grown p-GaN surface was smooth, with a surface roughness of 2.46 nm. After the Cl_2/Ar etch, the surface roughness increased to 4.30 nm, indicating plasma-induced damage roughening the surface. The UV/O_3 + HF treatment reduced the surface roughness to 2.08 nm, which is less than the as-grown GaN. It can be assessed that general damage is created from a plasma etch, roughening the surface, and that damage is recovered after UV/O_3 + HF treatment.

Photoluminescence (PL) was conducted across the series of p-GaN using a 325 nm wavelength He-Cd laser and can be seen in Figure 3. From the PL spectrum of the as-grown p-GaN, there is band edge emission at an energy of 3.36 eV. After the Cl_2/Ar etch the bandgap emission weakens and emission at 3.1 eV becomes the dominant transition. The 3.1 eV emission is likely due to donor-acceptor pair transitions created from plasma damage[19]. The post-etch treatment reduce the 3.1 eV emission source, indicating a reduction in the number of surface donor states from the damage. There is also a prominent 2.18 eV yellow luminescence (YL) band present, with the emission being strongest in the plasma etched sample but is reduced with treatment, being the smallest in the UV/O_3 + HF treatment.

Figure 3. Photoluminescence shows a degradation after the Cl_2+Ar etch and then a recovery of the original spectra after a UV/O_3 treatment.

Depth Resolved Cathodoluminescence Spectroscopy (DRCLS) was performed using an incident electron beam to generate a cascade of secondary electrons, and ultimately electron-hole pairs which recombine in band to band and band to deep level transitions on a near nanometer vertical scale[20]. Measurements were taken at a constant current of 2 mA while varying the beam energy from 0.5 kV to 3 kV to vary the depth of excitation on the surface of the p-GaN. Bohr-Bethe ranges from Monte Carlo simulations show that the maximum e-h recombination depth varies from 6nm to 90 nm at 0.5 kV to 3 kV beam energy.

Each spectrum is seen in Figure 4. Other than the NBE transition at 3.22 eV, two other transitions were observed at 2.0 eV and 2.51 eV. The 2.0 eV transition is likely related to carbon impurities[21], and the 2.51 eV transition is likely a nitrogen vacancy to Mg_{Ga} transition[22–24]. Each individual spectra was normalized to the NBE transition, by setting the intensity of the NBE to 1, allowing relative densities to be tracked as a function of beam energy, or recombination depth. To do this, spectra were deconvolved by fitting Gaussians to each transition. These areas are normalized against the areas of the NBE, allowing for relative densities to be compared between spectra and between samples.

Figure 4. Figure 4a., 4b., and 4c. shows DRCLS spectra for the as-received p-GaN, after a plasma etch, and after a UV/O_3 treatment respectfully. Each shows a segregation of defects towards the surface of the p-GaN. After a chlorine etch the defects within the first few nanometers increases, then decreases after a UV/O_3 + HF treatment. Figure 1d. shows the defect depth profile of the V_N.

Tracking the V_N as a function of depth shows a clear increase of surface defects after a plasma etch. The V_N acts as a donor in GaN so this will decrease the effectiveness for the p-type carriers. After subsequent damage treatment, surface defects decrease in the first few nanometers of the GaN. The UV/O_3 + HF treatment recovers the amount of V_N to levels even below the as-grown GaN. The temperature dependent I-V and DRCLS are likely referencing the same donor. The temperature dependent I-V showed a current leakage mechanism that had and a conduction band E_C – to - trap energy corresponding to E_C – 0.78 eV, and the DRCLS is showing a transition energy corresponding to E_C – ~0.9 eV. These are similar enough that it is likely the same donor state, a nitrogen vacancy[22–24].

In conclusion, Cl2 + Ar RIE plasma etching p-type GaN is likely increasing V_N density at the surface. The V_N acts as a donor, decreasing the effectiveness of the p-type GaN. Temperature dependent I-V found PFE at a state at E_C - ~0.78 eV. DRCLS found that there was an increase of V_N at the surface due to RIE plasma etching, that is recovered with a UV/O_3 + HF treatment. The V_N is seen to be E_C – ~0.9 eV, so that it is likely the V_N which the PFE is occurring through.Besides confirming the identity of the defects created by the ICP-RIE etch, these results show that these defects are limited to only the outer few nanometers, enabling their nearly 3-fold reduction by the UV ozone – HF treatment.

Acknowledgements

G.M. Foster acknowledges support from the American Society for Engineering Education (ASEE) postdoctoral fellow program. Work at the U.S. Naval Research Laboratory is supported by the Office of Naval Research. The authors are sincerely grateful to the following NRL Staff: Anthony Boyd, Walter Spratt, and Dean St. Amand for cleanroom equipment support.

LJB and BAN acknowledge support from AFOSR grant FA9550-18-1-0066 (Ali Sayir)

Work at Sandia was supported by Advanced Research Projects Agency – Energy monitored by Dr. Isik Kizilyalli. Sandia National Laboratories is a multimission laboratory managed and operated by National Technology & Engineering Solutions of Sandia, LLC, a wholly owned subsidiary of Honeywell International Inc., for the U.S. Department of Energy's National Nuclear Security Administration under contract DE-NA0003525.

Data Availability

The data that supports the findings of this study are available from the corresponding author upon reasonable request.

References:

[1] M.J. Tadjer, B.N. Feigelson, J.D. Greenlee, J.A. Freitas, T.J. Anderson, J.K. Hite, L. Ruppalt, C.R. Eddy, K.D. Hobart, and F.J. Kub, ECS J. Solid State Sci. Technol. **5**, P124 (2016).

[2] K. Nomoto, B. Song, Z. Hu, M. Zhu, M. Qi, N. Kaneda, T. Mishima, T. Nakamura, D. Jena, and H.G. Xing, IEEE Electron Device Lett. **37**, 161 (2016).

[3] C. Gupta, S.H. Chan, C. Lund, A. Agarwal, O.S. Koksaldi, J. Liu, Y. Enatsu, S. Keller, and U.K. Mishra, Appl. Phys. Express **9**, 8 (2016).

[4] Y.-J. Lin and Y.-L. Chu, J. Appl. Phys. **97**, 104904 (2005).

[5] M. Kato, M. Ichimura, E. Arai, and P. Ramasamy, Japanese J. Appl. Physics, Part 1 Regul. Pap. Short Notes Rev. Pap. **42**, 4233 (2003).

[6] K. Fu, J. Zhou, X. Deng, X. Qi, D.J. Smith, S.M. Goodnick, Y. Zhao, H. Fu, X. Huang, T.-H. Yang, C.-Y. Cheng, P.R. Peri, H. Chen, J. Montes, and C. Yang, IEEE J. Electron Devices Soc. **8**, 1 (2020).

[7] K. Fu, H. Fu, X. Huang, H. Chen, T.H. Yang, J. Montes, C. Yang, J. Zhou, and Y. Zhao, IEEE Electron Device Lett. **40**, 1728 (2019).

[8] S.J. Pearton, R.J. Shul, and F. Ren, MRS Internet J. Nitride Semicond. Res. **5**, e11 (2000).

[9] C.A. Carosella, B. Molnar, S. Schiestel, and J.A. Sprague, Mater. Res. Soc. Symp. - Proc. **595**, (2000).

[10] Yuhao Zhang, Min Sun, Hiu-Yung Wong, Yuxuan Lin, P. Srivastava, C. Hatem, M. Azize, D. Piedra, Lili Yu, T. Sumitomo, N.A. de Braga, R.V. Mickevicius, and T. Palacios, IEEE Trans. Electron Devices **62**, 2155 (2015).

[11] X.A. Cao, H. Cho, S.J. Pearton, G.T. Dang, A.P. Zhang, F. Ren, R.J. Shul, L. Zhang, R. Hickman, and J.M. Van Hove, Appl. Phys. Lett. **75**, 232 (1999).

[12] X.A. Cao, S.J. Pearton, A.P. Zhang, G.T. Dang, F. Ren, R.J. Shul, L. Zhang, R. Hickman, and J.M. Van Hove, Appl. Phys. Lett. **75**, 2569 (1999).

[13] A.P. Zhang, G. Dang, F. Ren, X.A. Cao, H. Cho, E.S. Lambers, S.J. Pearton, R.J. Shul, L. Zhang, A.G. Baca, R. Hickman, and J.M. Van Hoved, J. Electrochem. Soc. **147**, 719 (2000).

[14] A.D. Koehler, T.J. Anderson, M.J. Tadjer, B.N. Feigelson, K.D. Hobart, F.J. Kub, A. Nath, and D.I. Shahin, WiPDA 2016 - 4th IEEE Work. Wide Bandgap Power Devices Appl. 344 (2016).

[15] J.M. Shah, Y.L. Li, T. Gessmann, and E.F. Schubert, J. Appl. Phys. **94**, 2627 (2003).

[16] P. Fiorenza, G. Greco, F. Giannazzo, R. Lo Nigro, and F. Roccaforte, Appl. Phys. Lett. **101**, 172901 (2012).

[17] H. Schroeder, J. Appl. Phys. **117**, 215103 (2015).

[18] O. Mitrofanov and M. Manfra, J. Appl. Phys. **95**, 6414 (2004).

[19] T.W. Kang, S.H. Park, H. Song, T.W. Kim, G.S. Yoon, and C.O. Kim, J. Appl. Phys. **84**, 2082 (1998).

[20] G.M. Foster, G. Faber, Y.F. Yao, C.C. Yang, E.R. Heller, D.C. Look, and L.J. Brillson, Appl. Phys. Lett. **109**, (2016).

[21] A. Armstrong, A.R. Arehart, B. Moran, S.P. DenBaars, U.K. Mishra, J.S. Speck, and S.A. Ringel, Appl. Phys. Lett. **84**, 374 (2004).

[22] M.A. Reshchikov and H. Morkoç, J. Appl. Phys. **97**, 061301 (2005).

[23] M.A. Reshchikov, G.-C. Yi, and B.W. Wessels, Phys. Rev. B **59**, 13176 (1999).

[24] S. Hautakangas, J. Oila, M. Alatalo, K. Saarinen, L. Liszkay, D. Seghier, and H.P. Gislason, Phys. Rev. Lett. **90**, 137402 (2003).


(a)
As Fabricated
Two UV/O$_3$+HF Treatments
Reverse Current (A)
10^{-8}
10^{-9}
10^{-10}
10^{-11}
10^{-12}
10^{-13}
0
10
20
30
40
50
60
70
Reverse Voltage (V)
(b)
As Fabricated
Two UV/O$_3$+HF Treatments
n = 3.43
n = 2.57
Current (A)
10^{0}
10^{-1}
10^{-2}
10^{-3}
10^{-4}
10^{-5}
10^{-6}
10^{-7}
10^{-8}
10^{-9}
10^{-10}
10^{-11}
10^{-12}
10^{-13}
10^{-14}
0
1
2
3
4
5
Forward Voltage (V)
(c)
As Fabricated
Two UV/O$_3$+HF Treatment
Ideality Factor
6
5
4
3
2
1
2.0
2.5
3.0
Forward Voltage (V)

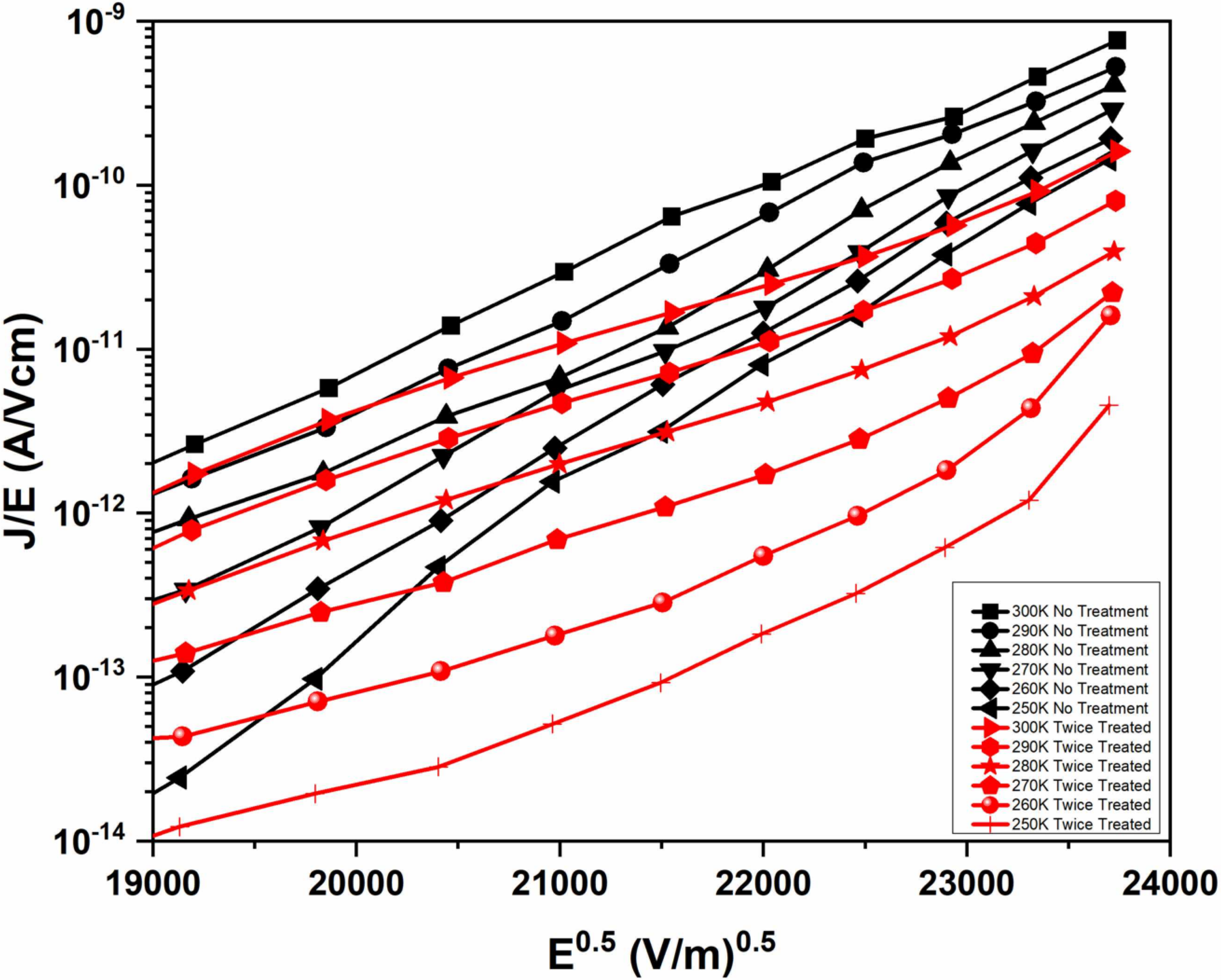
J/E (A/Vcm)
E^0.5 (V/m)^0.5
10^-9
10^-10
10^-11
10^-12
10^-13
10^-14
19000
20000
21000
22000
23000
24000
300K No Treatment
290K No Treatment
280K No Treatment
270K No Treatment
260K No Treatment
250K No Treatment
300K Twice Treated
290K Twice Treated
280K Twice Treated
270K Twice Treated
260K Twice Treated
250K Twice Treated

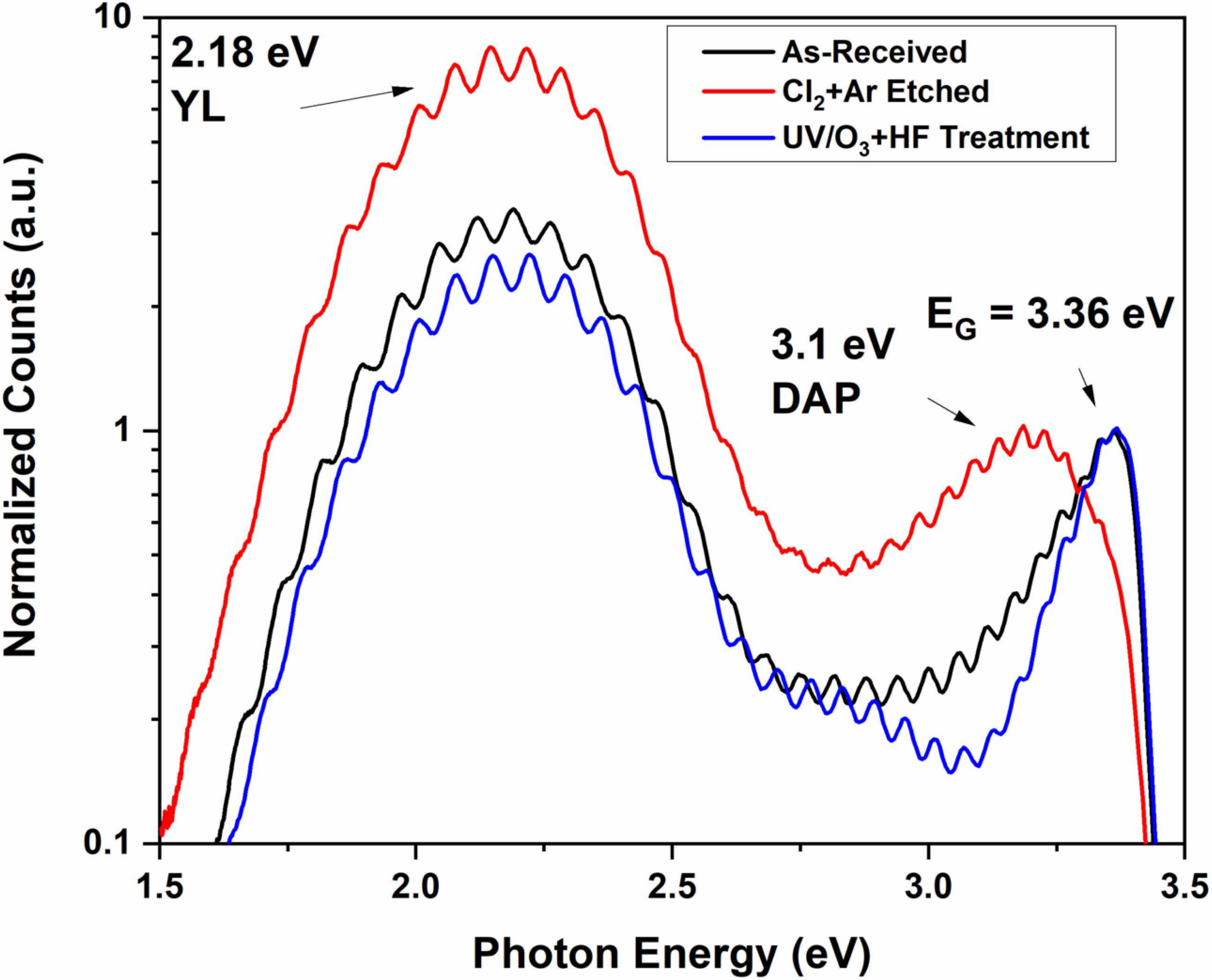
10
1
0.1
Normalized Counts (a.u.)
1.5
2.0
2.5
3.0
3.5
Photon Energy (eV)
2.18 eV
YL
3.1 eV
DAP
E_G = 3.36 eV
As-Received
Cl_2+Ar Etched
UV/O_3+HF Treatment

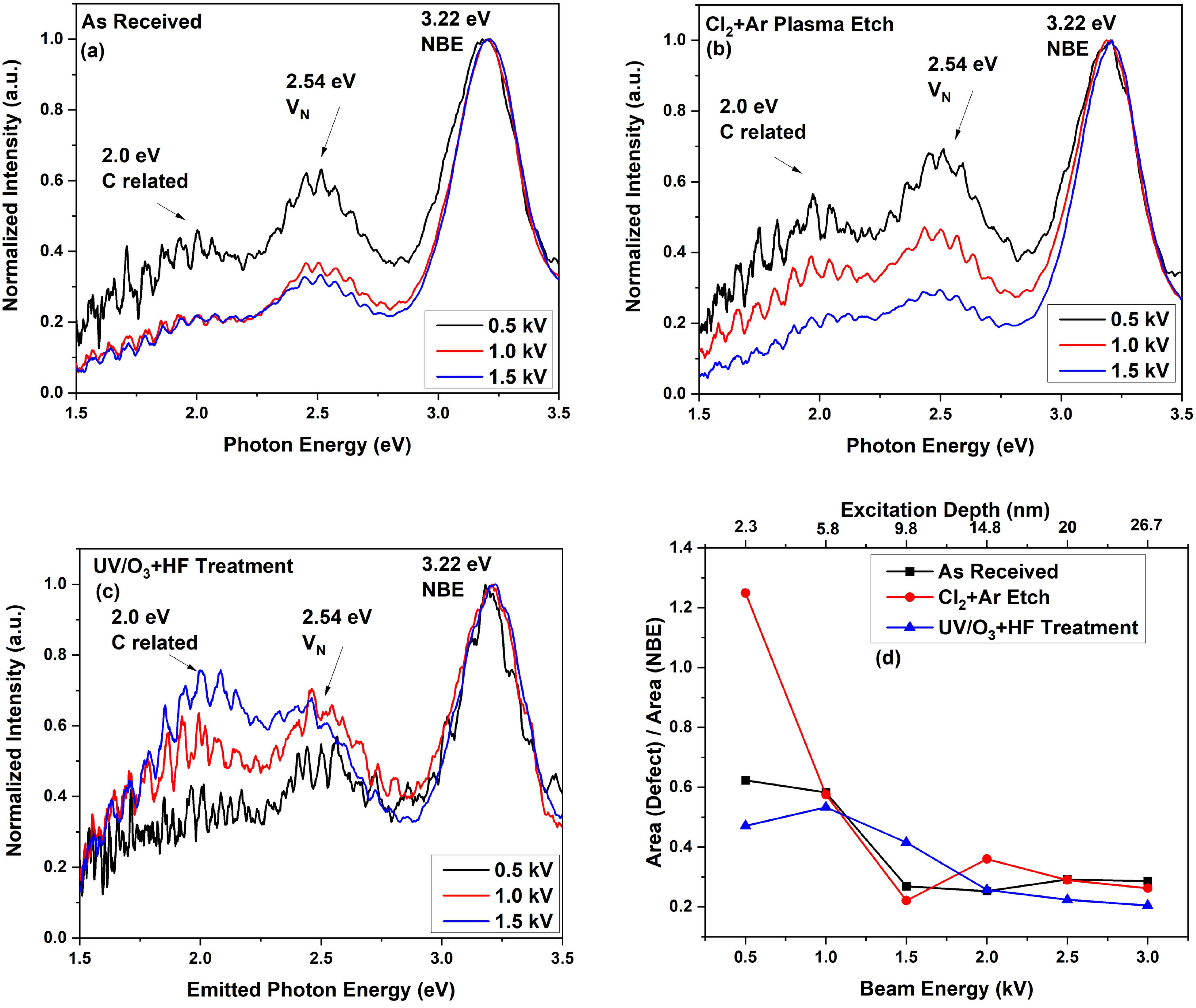
As Received
(a)
3.22 eV
NBE
2.54 eV
V_N
2.0 eV
C related
0.5 kV
1.0 kV
1.5 kV
Normalized Intensity (a.u.)
Photon Energy (eV)
0.0
0.2
0.4
0.6
0.8
1.0
1.5
2.0
2.5
3.0
3.5
Cl_2+Ar Plasma Etch
(b)
3.22 eV
NBE
2.54 eV
V_N
2.0 eV
C related
0.5 kV
1.0 kV
1.5 kV
Normalized Intensity (a.u.)
Photon Energy (eV)
UV/O_3+HF Treatment
(c)
2.0 eV
C related
2.54 eV
V_N
3.22 eV
NBE
0.5 kV
1.0 kV
1.5 kV
Normalized Intensity (a.u.)
Emitted Photon Energy (eV)
Excitation Depth (nm)
2.3
5.8
9.8
14.8
20
26.7
As Received
Cl_2+Ar Etch
UV/O_3+HF Treatment
(d)
Area (Defect) / Area (NBE)
0.2
0.4
0.6
0.8
1.0
1.2
1.4
Beam Energy (kV)
0.5
1.0
1.5
2.0
2.5
3.0